PAPER

How gravity and size affect the acceleration statistics of bubbles in turbulence

New Journal of Physics
The open-access journal for physics

How gravity and size affect the acceleration statistics of bubbles in turbulence

Vivek N Prakash[1,6], Yoshiyuki Tagawa[1], Enrico Calzavarini[2], Julián Martínez Mercado[1], Federico Toschi[3,4,5], Detlef Lohse[1,6] and Chao Sun[1,6]

[1] Physics of Fluids Group, Faculty of Science and Technology, J M Burgers Centre for Fluid Dynamics, University of Twente, PO Box 217, 7500-AE Enschede, The Netherlands
[2] Laboratoire de Mecanique de Lille CNRS/UMR 8107, Universite Lille 1–Science et Technologie and Polytech'Lille, Cite Scientifique Av. P Langevin, F-59650 Villeneuve d'Ascq, France
[3] Department of Physics, Eindhoven University of Technology, 5600-MB Eindhoven, The Netherlands
[4] Department of Mathematics and Computer Science, J M Burgers Center for Fluid Dynamics, Eindhoven University of Technology, 5600-MB Eindhoven, The Netherlands
[5] CNR-IAC, Via dei Taurini 19, I-00185 Rome, Italy
E-mail: v.n.prakash@utwente.nl, d.lohse@utwente.nl and c.sun@utwente.nl

New Journal of Physics **14** (2012) 105017 (14pp)
Received 19 July 2012
Published 19 October 2012
Online at http://www.njp.org/
doi:10.1088/1367-2630/14/10/105017

Abstract. We report the results of the first systematic Lagrangian experimental investigation in a previously unexplored regime of very light (air bubbles in water) and large ($D/\eta \gg 1$) particles in turbulence. Using a traversing camera setup and particle tracking, we study the Lagrangian acceleration statistics of $\sim$3 mm diameter (D) bubbles in a water tunnel with nearly homogeneous and isotropic turbulence generated by an active grid. The Reynolds number (Re_λ) is varied from 145 to 230, resulting in size ratios, D/η, in the range of 7.3–12.5, where η is the Kolmogorov length scale. The experiments reveal that gravity increases the acceleration variance and reduces the intermittency of the probability density function (PDF) in the vertical direction. Once the gravity

[6] Authors to whom any correspondence should be addressed.

1367-2630/12/105017+14$33.00

offset has been subtracted, the variances of both the horizontal and vertical acceleration components are about 5 ± 2 times larger than those measured in the same flow for fluid tracers. Moreover, for these light particles, the experimental acceleration PDF shows a substantial reduction of intermittency at growing size ratios, in contrast with neutrally buoyant or heavy particles. All these results closely match numerical simulations of finite-sized bubbles with the Faxén corrections.

Contents

1. Introduction

Suspensions of particulate materials, drops or bubbles carried by vigorously turbulent flows occur frequently both in the realm of natural phenomena (e.g. cloud formation) and in industrial applications (e.g. combustion in engines). In order to quantify the statistical properties of such suspensions, a prototype problem is often considered: the problem of a dilute suspension of spherical particles in incompressible, statistically homogeneous and isotropic turbulence [1, 2, 4]. In this simple form, the problem is defined by a set of three dimensionless parameters $[Re_\lambda, \Gamma, \Xi]$, respectively the Reynolds number based on the Taylor scale of the carrying flow, the particle to fluid mass density ratio ($\Gamma \equiv \rho_p/\rho_f$) and the particle to dissipative length ratio ($\Xi \equiv D/\eta$). Interesting theoretical questions concern how far the particle statistical properties (e.g. moments, probability density functions (PDFs), correlations) of position, velocity and acceleration depart from the Lagrangian properties of the fluid. The goal is to understand how such observables vary as a function of the control parameters.

Numerical studies have attempted to examine how closely the approximate equations of Lagrangian dynamics—which were known for a long time—are able to capture the dynamics. Since full numerics (e.g. physalis [5], front tracking [6]) are too expensive for high Re_λ, most simulations use a point particle (PP) model [7–9], also known as the Maxey–Riley–Gatignol model [10, 11]. In the real world, there are many situations where the particle size is larger than the Kolmogorov length scale of turbulence ($\Xi \gg 1$). Therefore, a large body of recent work ([3, 12–17]) has been dedicated to the characterization of these so-called *finite-sized* particles. Numerical simulations with Faxén corrections (FC) to the PP approach [14] correctly capture two important features from the experimental data for neutrally buoyant and heavy finite-sized

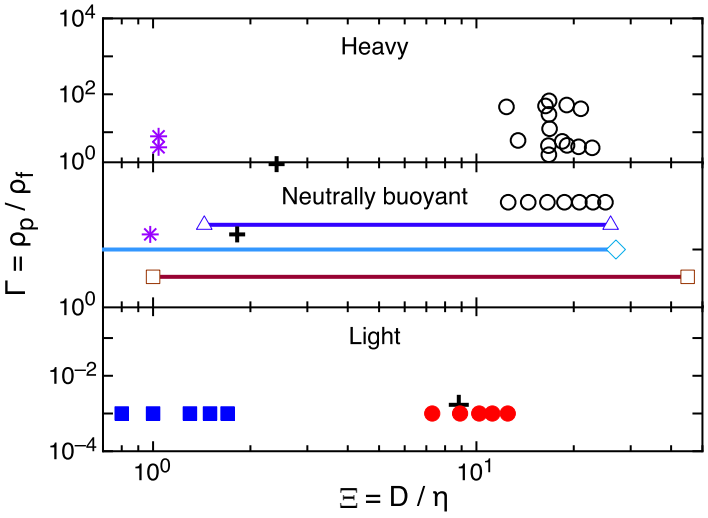

Figure 1. Parameter space of the density ratio versus size ratio for particles in turbulence, from the data available in the literature: △, Voth *et al* [3]; ○, Qureshi *et al* [13]; +, Volk *et al* [19]; ◇, Brown *et al* [15]; ∗, Gibert *et al* [16]; □, Volk *et al* [17]; ■, Martínez Mercado *et al* [20]; and ●, the present work. Most of the previous studies have focused on $\Gamma \geqslant 1$, and here we explore the $\Gamma \ll 1$ case.

particles [3, 12, 13, 15–17]: the acceleration PDF of the finite-sized particles, in general, show less intermittency than those of fluid tracers; and their acceleration variance decreases with increasing size ratio. However, for light particles ($\Gamma < 1$), the Faxén corrected numerics [14] remarkably indicate an opposite trend for the acceleration statistics at growing Ξ: an initial increase of acceleration variance and intermittency, followed by a decrease. These predictions for light particles are awaiting experimental verification.

However, these experiments are highly challenging in terms of the infrastructure needed, techniques and analysis, but are of great importance for a fundamental understanding of particles in turbulence.

In this paper, we present the first systematic experimental investigation in the regime ($\Gamma \ll 1$, $\Xi > 1$) of the parameter space, i.e. very light and large particles (see figure 1 for a summary of all the currently available measurements). For such an investigation, we use air bubbles, which are dispersed in a turbulent water flow. We track these bubbles using a traversing camera system which can perform two-dimensional (2D) recordings of the vertical and one horizontal component of the bubble trajectories. The experiments are compared to numerical simulations based on the particle Lagrangian equations with Faxén correction [14]. We also experimentally study the effects of gravity, as it could be important at lower Re_λ, and very few numerical studies [18] have taken gravity into account.

The paper is organized as follows. In section 2, we describe in detail the experimental setup (section 2.1), the bubble deformability and size distribution (section 2.2). Next, we present results on the velocity statistics (section 3) and the acceleration statistics (section 4). The effects of gravity and size on the acceleration statistics are discussed in sections 4.1 and 4.2, followed by the conclusions in section 5.

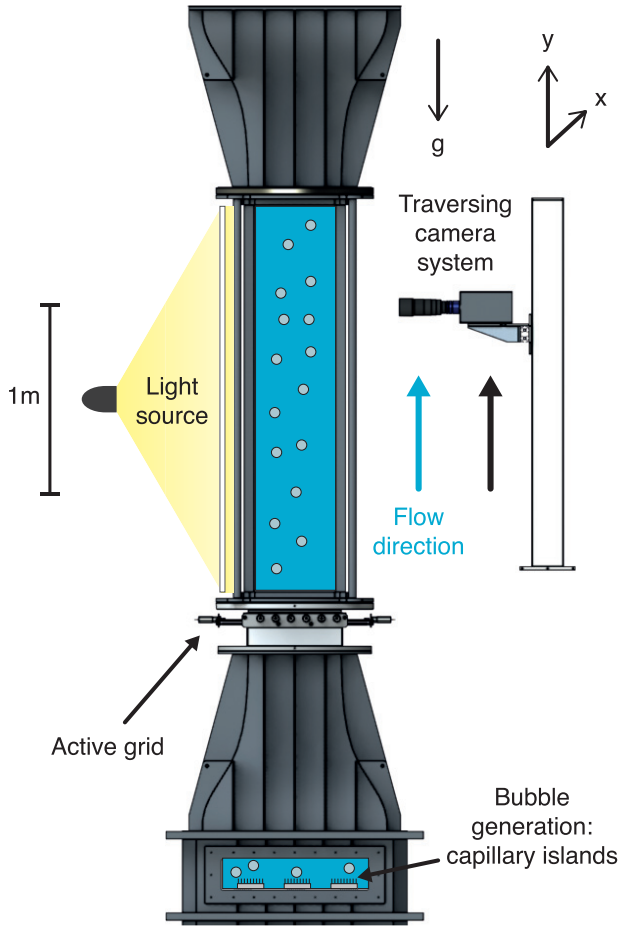

Figure 2. The TWT facility: vertical water tunnel with nearly homogeneous and isotropic turbulence generated by an active grid. Bubbles are dispersed from below through capillary islands and the flow is in the upward direction. The camera moves upward at preset speeds, along with the bubbles, allowing the measurement of long-duration trajectories.

2. Experiments and analysis

2.1. Experimental setup

In our experiments, air bubbles in water, $\Gamma \approx 10^{-3}$, are dispersed in a turbulent flow in the 8 m high Twente Water Tunnel (TWT) facility (see figure 2(a)). Nearly homogeneous and isotropic turbulence is generated by the flow of water through an active grid [21]. An optically transparent measurement section of dimensions $2 \times 0.45 \times 0.45\,\mathrm{m}^3$ is located downstream of the active grid. We recently reported the results on $\sim$0.3 mm diameter bubbles [20, 22] using the same experimental facility (see also [23, 24]). Here, one important modification is made: the position of the active grid is switched from the position on top of the measurement section to its bottom. Furthermore, the direction of the water flow through the active grid is now upwards. The bubbles are generated by blowing air through capillary islands (diameter 500 μm) placed below the active grid. The bubbles rise through the measurement section along with the imposed

water flow and escape through an open vent on top of the water tunnel. A surfactant (Triton X-100) is added to the tap water to reduce the bubble deformability [25] (more details follow in section 2.2). Re_λ is varied from 145 to 230 by changing the mean flow speed of water in the tunnel. The flow characterization is done using a hot-film probe placed in the center of the measurement volume [20]. The 2D Lagrangian particle tracking experiments are carried out using a high-speed camera (Photron SA1.1) at an image acquisition rate of 5000 frames per second (fps) with a resolution of 768×768 pixels. The camera is focused on a 1–2 cm thick plane in the middle of the measurement section and the illumination is provided from the opposite side by a halogen light source placed behind a diffusive plate. The camera is mounted on a traverse system (Aerotech L-ATS62150 linear stage) which enables precise movement in the vertical direction at preset velocities.

The detection of the bubble centers in the images is a non-trivial task because the bubbles often overlap or go out of focus (see figure 2(b)). However, the circular Hough transform method [27] is successfully used to detect more than 90% of the bubbles (which are in focus) in the images. The Hough transform is a technique for extracting features in images, and has been used widely in the field of computer vision and digital image processing. During image processing, edge-detection algorithms are used to extract attributes from images, and these are followed by linking procedures (such as the Hough transform) to assemble edge pixels into useable edges [28]. Initially, the technique was used for line detection and then extended to circles and ellipses and eventually to arbitrary shapes [29].

A 2D particle tracking code is used to obtain the bubble trajectories over time. The data processing approach is the same as that in the work by Martínez Mercado *et al* [20]. The fitting window lengths (N) of the trajectory smoothing for the microbubble experiments (see [20] for more details) and the present experiments have been chosen to be consistent. The fitting window length is $N = 15$ for the present experiments at 5000 fps acquisition rate and $N = 30$ for the microbubble experiments at 10 000 fps acquisition rate.

2.2. *Bubble deformability and size distribution*

A surfactant (Triton X-100) is added to the tap water to reduce the bubble deformability. The small amount of surfactant (< 1 ppm) used in the present experiments is much below the critical micelle concentration, so the change in flow properties is negligible [26]. Although the addition of surfactant reduces the surface tension by a few per cent, it leads to another competing effect, namely the suppression of bubble coalescence at the source of injection. This second effect is more dominant and as a result we see a reduction of the bubble size [25].

Figure 3 shows the difference between bubbles in tap water and in a surfactant solution. We clearly see a big difference in the shapes and sizes of the bubbles. The deformation is greatly reduced in the presence of surfactant, thanks to the smaller size. Nonetheless, in figure 3, the bubbles still appear to be deformed and anisotropic, but the effect is much less than without surfactants: the addition of surfactants leads to a *reduced* deformability of the bubbles and not to a perfect spherical shape. The principal-axis deformation ratios, defined as b/a, where a, b are the major and minor axis lengths of the best-fitting ellipse, are more than $1/2$. For example, the deformation ratio in the case of $Re_\lambda = 170$ ($\Xi = 8.9$) is 0.75 ± 0.15—which indicates small deformability, approaching a circle. The images in figure 3 are instantaneous snapshots from the experiments. It must be noted that the deformation of real bubbles is strongly time dependent, and the addition of surfactant significantly reduces this deformation over time. Thus,

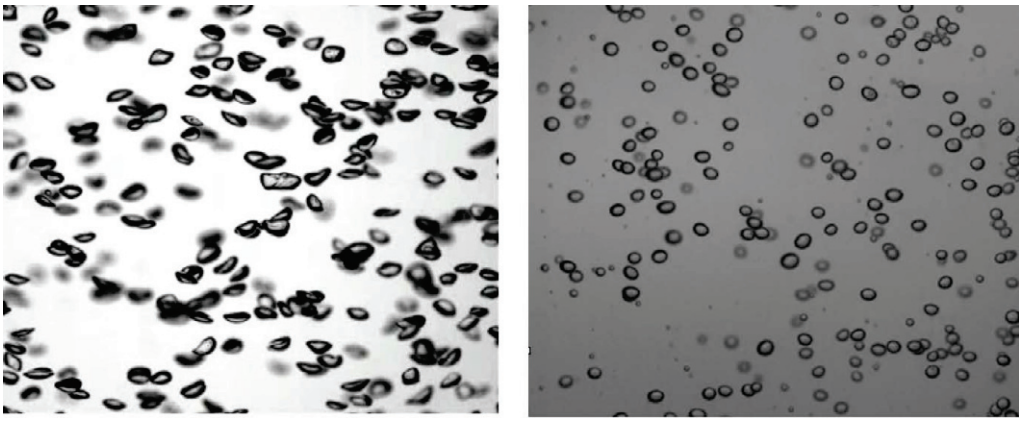

Figure 3. Left panel: rising bubbles of diameter ∼5 mm in tap water. Right panel: bubbles of diameter ∼ 3 mm in surfactant solution (with < 1 ppm Triton X-100).

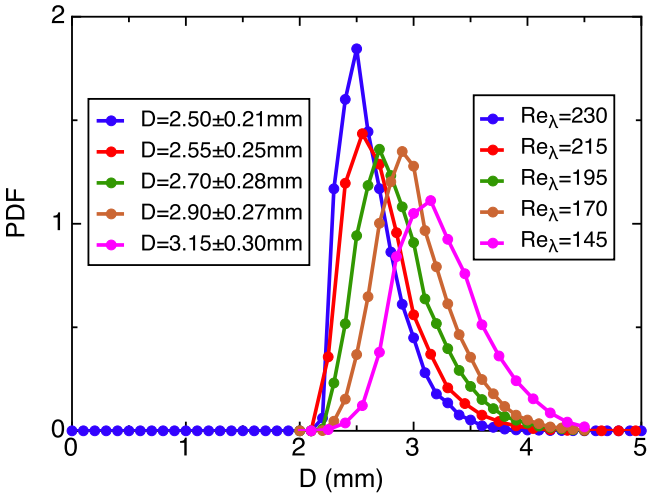

Figure 4. Distribution function of bubble diameters, D, at different Re_λ.

the addition of the surfactant renders the images amenable to processing, which is otherwise a nearly impossible task.

The bubble diameter has a weak dependence on Re_λ, as shown in figure 4. We select the peak values of the distribution as the characteristic bubble diameter; $D = 3.15$, 2.90, 2.70, 2.55 and 2.50 mm (with absolute deviations $\sim\pm 0.3$ mm, see figure 4) at $Re_\lambda = 145$, 170, 195, 215 and 230, respectively. This variation in Re_λ changes the Kolmogorov length scale (η), and the corresponding size ratios are $\Xi = 7.3$, 8.9, 10.2, 11.2 and 12.5.

3. Results—velocity statistics

In the present experiments, the bubble motion and liquid mean flow are both upwards. The terminal velocity of the ∼3 mm bubbles in the absence of a liquid mean flow (still liquid) is determined from our experiments to be 25 cm s^{-1}. In the presence of a liquid mean flow, the

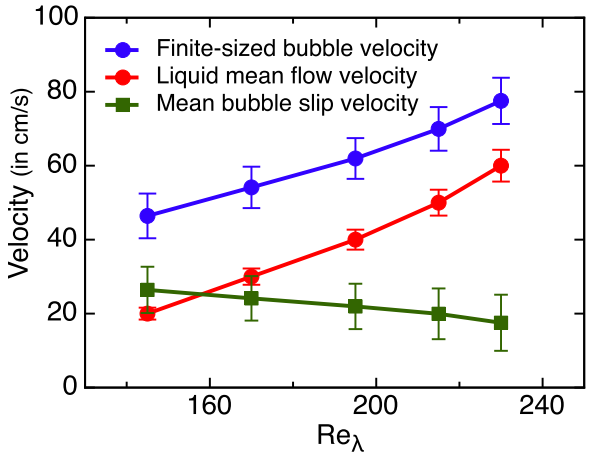

Figure 5. Finite-sized bubble slip velocity at different Re_λ.

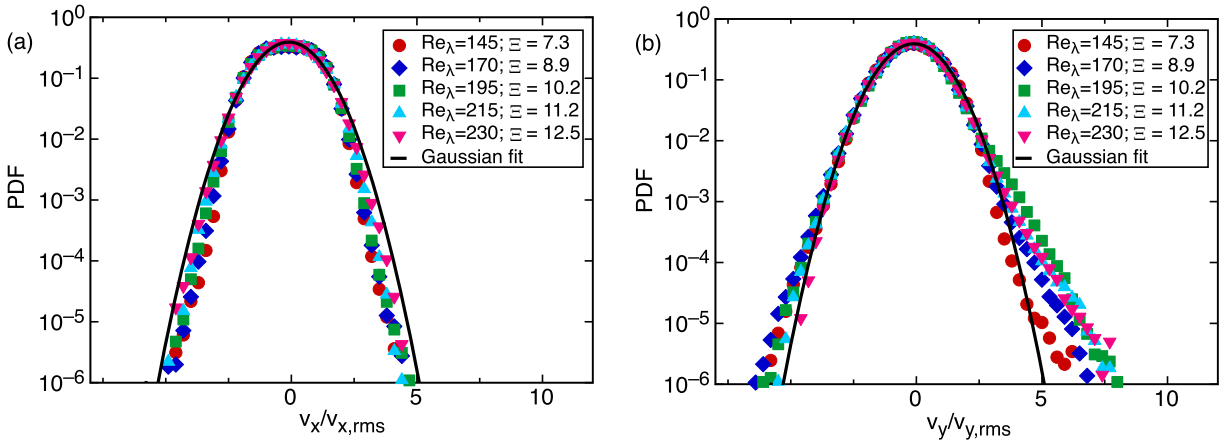

Figure 6. Velocity PDFs of the finite-sized bubbles at different Re_λ (and Ξ): (a) horizontal component, v_x; (b) vertical component, v_y. The solid line in panels (a) and (b) represents a Gaussian distribution fit. The velocity PDF in (a) is mostly sub-Gaussian, and in (b) we see more intermittency than a Gaussian profile.

bubbles attain their terminal velocity and then feel the turbulence of the surrounding liquid flow. In figure 5, we show the actual mean rise velocities of the bubbles (measured from the present experiments) compared to the liquid mean flow speeds. The bubbles experience a so-called 'slip' and are able to rise with velocities higher than the liquid mean flow. We quantify this 'mean bubble slip velocity' by defining it as the difference between the bubble rise velocity and the liquid mean flow velocity. The variation of this mean slip velocity with Re_λ is shown in figure 5. We observe that the mean bubble slip velocity decreases with an increase in Re_λ. This decreasing trend might be due to the decreasing bubble size at higher Re_λ.

We now present here results on the PDFs of the finite-sized bubble velocity obtained from the present experiments. Figures 6(a) and (b) show the PDF of the horizontal (x) and vertical (y) components of the normalized bubble velocity at the different Re_λ (and Ξ) covered in the present study. We observe that the x-component velocity distributions (figure 6(a)) follow

sub-Gaussian statistics (flatness values: 2.27–2.78) and the y-component velocity distributions (figure 6(b)) show a slightly higher intermittency compared to the Gaussian profile (flatness values: 2.89–3.77). The vertical component velocity distributions are also asymmetric, owing to the effects of gravity. In previous experiments on finite-sized neutrally buoyant particles in turbulent von Kármán flows, Volk *et al* [17] obtained sub-Gaussian velocity distributions with flatness around 2.4–2.6, but in the past, Gaussian-type flatness values (2.8−3.2) were also reported [3]. The reason for the deviations of the velocity distributions from Gaussianity is still an open question.

4. Results—acceleration statistics

4.1. Acceleration statistics: gravity effect

We first address the effect of gravity on the acceleration statistics. Since the buoyancy is proportional to bubble volume, while the laminar viscous drag grows with the linear size of the bubble, it is clear that for growing bubble sizes and fixed turbulence intensity (growing Ξ), buoyancy at some point shall dominate. The opposite is true for the case of fixed bubble size but increasing Reynolds numbers (again growing Ξ) in our experiments, where buoyancy loses its dominance at higher Re_λ. In summary, it is acceptable to neglect the buoyancy force only for small bubbles $\Xi \lesssim 1$ [20] or for large Re_λ, as we find later.

One may expect that the buoyancy force will produce *asymmetry* on the vertical component statistics because buoyancy will add on to the upward acceleration events and will subtract from the downward events. However, we find that the asymmetry is almost negligible. Firstly, we find that the mean value of the vertical component of acceleration (y) is essentially zero, as it is for the horizontal one (x): $\langle a_x \rangle \simeq \langle a_y \rangle = 0 \pm 0.2\, g$, where g is the acceleration due to gravity. Secondly, we observe that the PDF shape is only very weakly asymmetric; we indeed estimate the skewness, $S(a_i) \equiv \langle a_i^3 \rangle / \langle a_i^2 \rangle^{3/2}$, and find that $|S(a_x)| \leqslant 0.01$ and $|S(a_y)| \leqslant 0.1$. The skewness is comparable to the values found for $\Xi < 2$ bubbles (from now on called microbubbles) studied in the same setup [20]. We can conclude that if any asymmetry is present it must be very weak.

The buoyancy force, however, produces a robust *anisotropy*: different statistics for the vertical and horizontal acceleration components. This influence of gravity is clearly visible in the second statistical moments of acceleration, shown in figure 7(a), where the variance $\langle a_i^2 \rangle$ is plotted. We find that $\langle a_y^2 \rangle \gg \langle a_x^2 \rangle$ for all $\Xi > 7.3$ bubbles, while from the same figure it is evident that microbubbles have much closer variance values for the three Cartesian components. If one calls a_y' the vertical acceleration component in the absence of gravity and assumes that $\langle a_y^2 \rangle = \langle (a_y' - g)^2 \rangle$, one obtains $\langle a_y'^2 \rangle = \langle a_y^2 \rangle - g^2$, since $\langle a_y' \rangle = 0$ because of isotropy. As can be seen from figure 7(a), this produces a reasonable collapse of the x–y data $\langle a_y^2 \rangle - g^2 \simeq \langle a_x^2 \rangle$. We emphasize that the collapse observed for the second-order moment is non-trivial. It means that the statistical effect of gravity seems to be additive on the vertical direction with no effect on the horizontal component. An immediate consequence is that the effect of the hydrodynamic forces coupling different Cartesian directions, such as for example the lift force, turns out to be unimportant here.

As mentioned above, we found that the acceleration variance $\langle a_y^2 \rangle$ in the vertical direction is augmented by an offset (or a correction factor) that depends on g^2. Although we found that the offset of $\sim g^2$ seems to work well for the present finite-sized bubbles, we do not yet have

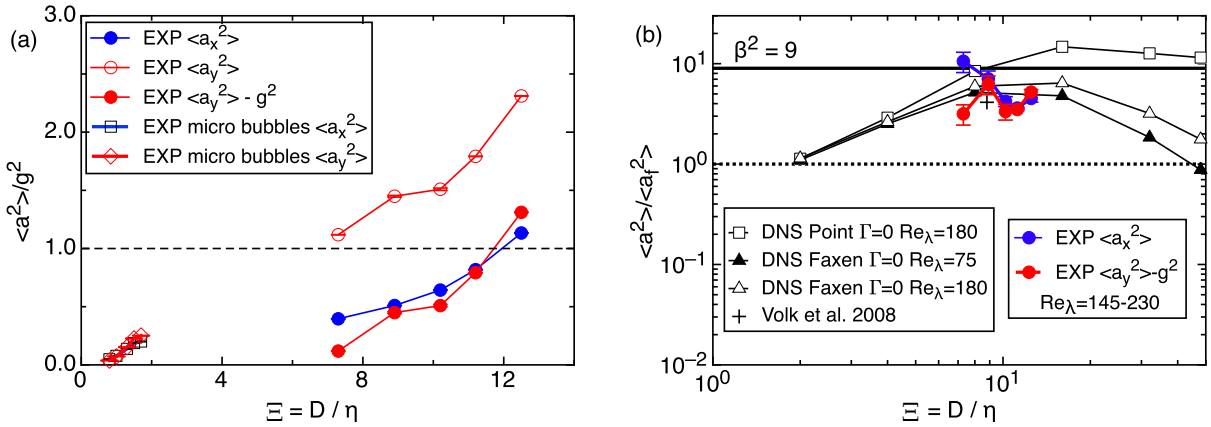

Figure 7. (a) The single-component acceleration variance normalized by the gravitational acceleration for large bubbles and microbubbles [20]. (b) The normalized acceleration variance versus the size ratio. Legend: the present large bubble results (•) are represented with error bars, along with a gravity offset for the vertical component a_y. (□): PP DNS of bubbles [14]; (△ and ▲): bubbles from DNS with FCs [14]; (+): single experimental point for bubbles [19].

a physical understanding of the origin of this correction. When one examines the equations governing the motion of bubbles in a turbulent flow (Maxey–Riley–Gatignol equations) [10, 11] including gravity, the corresponding acceleration variance offset would then be $\sim 4g^2$, which does not work for the present data. Clearly, there seems to be a complex interplay between gravity and inertia, and more experimental and numerical work is needed before we can arrive at a solid conclusion on the gravity correction factor. These corrections will be explored in detail in future work.

The finite-sized bubble acceleration PDFs and the flatness values at two selected cases of Re_λ are shown in figure 8. The quality of statistics in the present experimental data is seen in the insets of figures 8(a) and (b), which demonstrate that the fourth-order moments are well converged. Hence, we can calculate the flatness directly from the distribution without resorting to a fitting procedure (e.g. as in Volk *et al* [17]). In figure 8(c), we observe that the flatness values of a_y at $Re_\lambda \leqslant 195$ are less than those of a_x. At higher Re_λ ($\geqslant 215$), the flatness values of a_x and a_y become comparable, and the corresponding PDFs show a nice collapse in figure 8(b). The decreased intermittency in the vertical component a_y for the low Re_λ (seen in figure 8(a)) is due to gravity. Apparently, there are two regimes: at lower Re_λ, gravity has an effect on the acceleration statistics in the vertical direction, which is no longer the case at higher Re_λ.

4.2. Acceleration statistics: size effect

Once the statistical influence of buoyancy has been disentangled, we can now study how the gravity-less acceleration variance changes at increasing Ξ; in other words we study the purely hydrodynamic size effect on particles that are lighter than the surrounding fluid. It is convenient to look at the relative change of the bubble acceleration variance with respect to fluid tracers $\langle a_{i,f}^2 \rangle$. For $a_{i,f}$ we use here the acceleration of the microbubbles as found in [20], because given their small size, $\Xi < 2$, they behave almost like Lagrangian tracers. Furthermore, the Re_λ

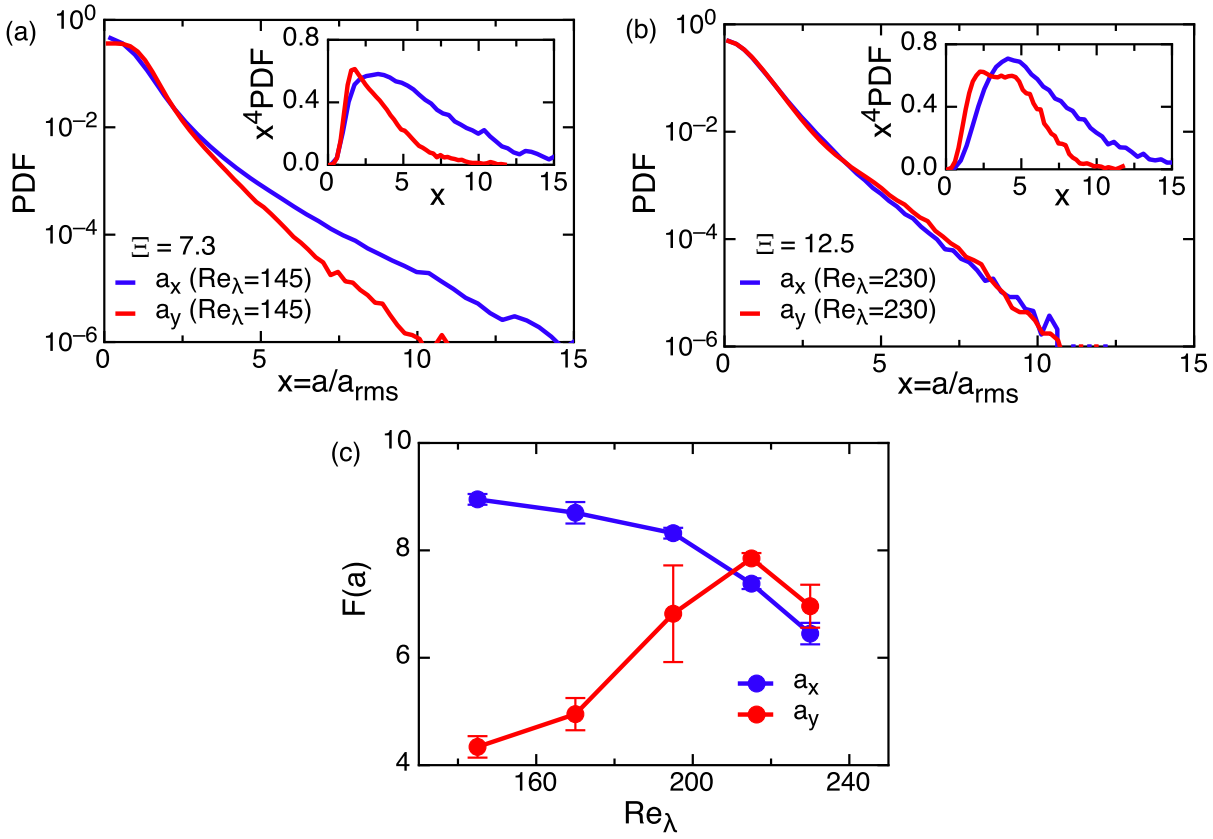

Figure 8. Normalized bubble acceleration PDFs of a_x and a_y components at $Re_\lambda =$ (a) 145 and (b) 230, which are respectively the smallest and largest Re_λ considered in our experiments. As expected, at the lower Re_λ the tails of the normalized PDF (in other words the flatness) of the vertical component are reduced compared to the horizontal one, while at the higher Re_λ the anisotropy is negligible. The insets in (a) and (b) show the fourth-order convergence test. (c) The acceleration flatness for the present bubbles (with error bars) versus Re_λ.

numbers studied in the present experiments are very close to those analyzed in [20] and the flow conditions are the same. Figure 7(b) reports such a normalized acceleration variance $\langle a_i^2 \rangle / \langle a_{i,f}^2 \rangle$ versus the size ratio Ξ. We see that both acceleration components reach a level of 5 ± 2 times the variance measured in the same flow for fluid tracers. They are also in agreement with the previous single experimental data point of [19]. To get an interpretation of this measurement, we compare it with the results of numerical simulations at similar Re_λ. Figure 7(b) reports the results of two different types of Lagrangian particle simulations, first the so-called point-particle (PP) simulation that only takes into account the hydrodynamic effects of added mass and Stokes drag, and a second simulation that adds Faxén corrections (FCs) to the mentioned terms [14, 30]. The PP model predicts for $\Xi \to \infty$ an asymptotic limit of normalized acceleration variance which is nine times that for tracers (as a result of the dominance of the added-mass term). From figure 7(b), we deduce that for $\Xi \approx 10$ in the PP model, it is about 15 times the value for tracers, reflecting that we are not yet in the asymptotic limit. For larger Ξ, the results of the PP model indeed seem to approach the asymptotic value of normalized acceleration variance of 9. FCs to

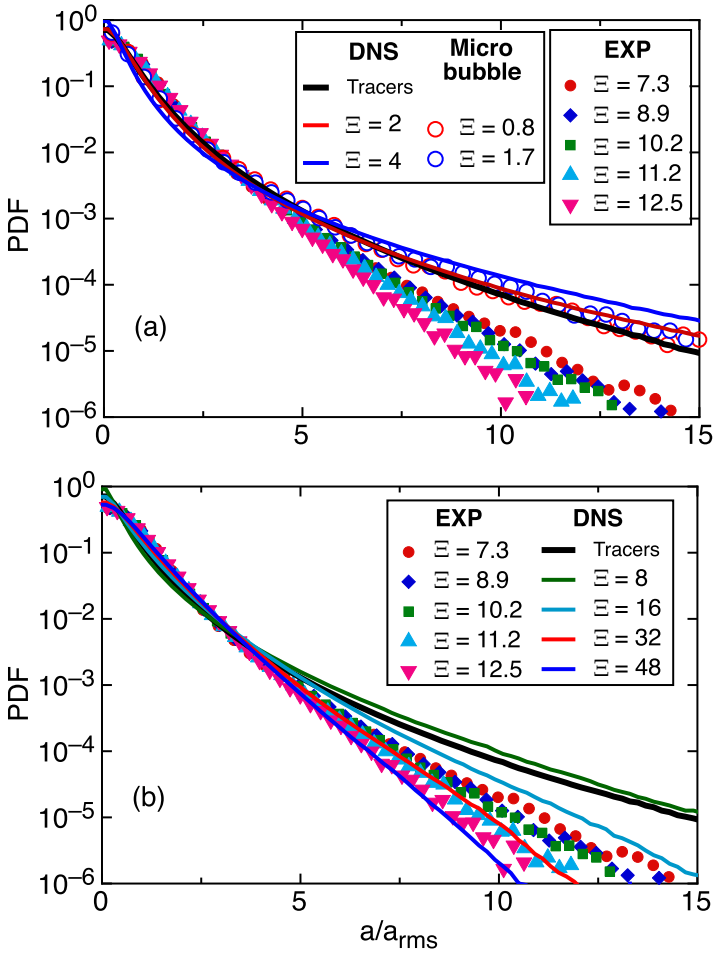

Figure 9. The normalized acceleration PDFs of the horizontal component $|a_x|$, from the present bubble experiments (EXP), microbubble measurements [20] and numerical simulations (DNS) with the Faxén model at $Re_\lambda = 180$ [14]. (a) Comparison with the results for point-like particles: DNS tracers, microbubbles and Faxén DNS of bubbles for $\Xi \leqslant 4$. (b) Comparison with Faxén DNS of larger bubbles, $\Xi \geqslant 8$.

the added mass term reduce the value at $\Xi = 10$ which is about 7. Figure 7(b) clearly shows that numerical simulations of Faxén corrected finite-sized bubbles show good agreement with the experimental measurements (in contrast to the PP model that overestimates the result). The present results are the first systematic measurements to confirm that the acceleration variance increases with finite size for bubbles, matching the FC numerical simulations [14]. Note again that the trend is very different for the case of neutrally buoyant particles and heavy particles, for which the normalized acceleration variance is always $\leqslant 1$ [14, 17]. It must also be noted that the acceleration statistics have not been found to show appreciable changes for $\Xi < 5$ in experiments [3, 15, 20] and for $\Xi < 2$ in numerics [14]. Hence, the numerical results are only shown in the regime $\Xi > 2$, where the FCs start playing a role.

Making statements on the fourth order statistical moments of acceleration based on experimental measurements is a delicate endeavor; see, e.g., the detailed analysis by Volk *et al* [19]. To study the finite-size effects on the bubble acceleration, in the following we will

focus on the PDF shape of the normalized x-acceleration, $a_x/\langle a_x\rangle_{\rm rms}$, which is not directly affected by gravity. In figure 9(a), first we plot such a curve for microbubbles [20] and see that its shape falls on that for fluid tracers and on $\Xi < 2$ bubbles, from DNS at a similar Re_λ. This is evidence of both the above-mentioned passive nature of microbubbles and of the similarity between turbulence realized in the Twente Channel flow and that produced in homogeneous and isotropic DNS. In the same panel, we see that, in sharp contrast, the finite-sized bubbles show a strongly reduced intermittency. This is the first time that such a substantial change in intermittency at growing size ratios was experimentally observed: neither for solid neutrally buoyant particles [15, 17] nor for heavier bubbles [13] was it detected previously.

In order to clarify further the magnitude of such an effect, in figure 9(b) we compare the acceleration PDF from the DNS simulations with FCs and the present experiments. There is an initial increase of flatness in the DNS simulations for $\Xi \lesssim 8$, which probably reflects the limitations of the FCs. For $\Xi \gtrsim 7$–8 both the numerics and the experiments show a significant reduction of the tails of the PDF. However, the DNS appears to underestimate its functional behavior by approximately a factor of 2–3 in the size parameter Ξ. The reason for this discrepancy is currently unclear. One reason could be that the simulations neglect the two-way coupling and are just approximated in the implementation of Faxén terms. Another possible reason for the discrepancy which deserves further study is the deformability of real bubbles. The deformation process absorbs/releases energy from/to the turbulent environment, a process that may have an effect on acceleration statistics. These issues motivate further investigations to better understand light particles in turbulence.

5. Conclusion

We carried out measurements of Lagrangian acceleration in the previously unexplored regime of large (compared to η) and very light (with respect to ρ_f) particles in turbulence. Bubbles of size $\sim$3 mm diameter (D) were tracked in turbulent flow conditions in a water tunnel. The explored ranges of Reynolds number (Re_λ) and size ratios, $\Xi = D/\eta$, were 145–230 and 7.3–12.5, respectively.

Gravity produces anisotropy in the acceleration statistics of the vertical component—it adds a g^2 offset to the variance, and decreases the intermittency of PDF, at lower Re_λ. It was found that the interaction between gravity and inertia is complex, and this deserves further study.

The acceleration variances clearly indicate the finite-size effect, and the results are in good agreement with DNS simulations with the Faxén corrections. The intermittency of experimental PDF decreases with increasing Ξ. However, the PDF obtained from the Faxén corrected numerics shows a difference of factor $\sim$2–3 in Ξ compared to the experiments. The reason for this discrepancy between numerics and experiments deserves further study. To improve the current understanding, we plan to study in the future rigid hollow spheres in the turbulent water flow and to vary their diameters, D, at fixed Re_λ numbers.

Acknowledgments

We are grateful to the *New Journal of Physics* guest editors (M Bourgoin and H Xu) who invited us to submit this work. We thank G Voth, L-P Wang, H Xu and B Luethi for discussions and G-W Bruggert, M Bos and B Benschop for help with the experimental setup. We also thank J van Nugteren and B Colijn for assistance with the experiments. FT and CS attended the New

Directions in Turbulence program at the Kavli Institute for Theoretical Physics China (KITPC) supported by the Project of Knowledge Innovation Program (PKIP) of Chinese Academy of Sciences, Grant No. KJCX2.YW.W10. JMM acknowledges support from the Foundation for Fundamental Research on Matter (FOM) through the FOM-IPP Industrial Partnership Program: 'Fundamentals of heterogeneous bubbly flows'. We also acknowledge support from the European Cooperation in Science and Technology (COST) Action MP0806: 'Particles in turbulence'. Finally, we thank two anonymous referees for their constructive comments.

References

[1] Toschi F and Bodenschatz E 2009 Lagrangian properties of particles in turbulence *Annu. Rev. Fluid Mech.* **41** 375

[2] La Porta A, Voth G, Crawford A M, Alexander J and Bodenschatz E 2001 Fluid particle accelerations in fully developed turbulence *Nature* **409** 1017

[3] Voth G, La Porta A, Crawford A M, Alexander J and Bodenschatz E 2002 Measurement of particle accelerations in fully developed turbulence *J. Fluid Mech.* **469** 121

[4] Lohse D 2008 Particles go with the flow *Physics* **1** 18

[5] Prosperetti A and Oguz H N 2001 Physalis: a new o(N) method for the numerical simulation of disperse systems: potential flow of spheres *J. Comput. Phys.* **167** 196

[6] Tryggvason G, Bunnerm B, Esmaeeli A, Juric D, Al-Rawahi N, Tauber W, Han J, Nas S and Jan Y-J 2001 A front-tracking method for the computations of multiphase flow *J. Comput. Phys.* **169** 708

[7] Arneodo A *et al* 2008 Universal intermittent properties of particle trajectories in highly turbulent flows *Phys. Rev. Lett.* **100** 254504

[8] Volk R, Calzavarini E, Verhille G, Lohse D, Mordant N, Pinton J-F and Toschi F 2008 Acceleration of heavy and light particles in turbulence: comparison between experiments and direct numerical simulations *Physica* D **237** 2084

[9] Biferale L, Bodenschatz E, Cencini M, Lanotte A S, Ouellette N T, Toschi F and Xu H 2008 Lagrangian structure functions in turbulence: a quantitative comparison between experiment and direct numerical simulation *Phys. Fluids* **20** 065103

[10] Maxey M R and Riley J J 1983 Equation of motion for a small rigid sphere in a nonuniform flow *Phys. Fluids* **26** 883

[11] Gatignol R 1983 The Faxèn formulae for a rigid particle in an unsteady non-uniform Stokes flow *J. Mec. Theor. Appl.* **1** 143

[12] Qureshi N M, Bourgoin M, Baudet C, Cartellier A and Gagne Y 2007 Turbulent transport of material particles: an experimental study of finite size effects *Phys. Rev. Lett.* **99** 184502

[13] Qureshi N M, Arrieta U, Baudet C, Cartellier A, Gagne Y and Bourgoin M 2008 Acceleration statistics of inertial particles in turbulent flow *Eur. Phys. J.* B **66** 531

[14] Calzavarini E, Volk R, Bourgoin M, Leveque E, Pinton J-F and Toschi F 2009 Acceleration statistics of finite-sized particles in turbulent flow: the role of Faxèn forces *J. Fluid Mech.* **630** 179

[15] Brown R D, Warhaft Z and Voth G A 2009 Acceleration statistics of neutrally buoyant spherical particles in intense turbulence *Phys. Rev. Lett.* **103** 194501

[16] Gibert M, Xu H and Bodenschatz E 2010 Inertial effects on two-particle relative dispersion in turbulent flows *Europhys. Lett.* **90** 64005

[17] Volk R, Calzavarini E, Leveque E and Pinton J-F 2011 Dynamics of inertial particles in a turbulent von Kármán flow *J. Fluid Mech.* **668** 223

[18] Mazzitelli I and Lohse D 2004 Lagrangian statistics for fluid particles and bubbles in turbulence *New J. Phys.* **6** 203

[19] Volk R, Mordant N, Verhille G and Pinton J-F 2008 Laser Doppler measurement of inertial particle and bubble accelerations in turbulence *Europhys. Lett.* **81** 34002

[20] Martínez Mercado J, Prakash V N, Tagawa Y, Sun C and Lohse D 2012 Lagrangian statistics of light particles in turbulence *Phys. Fluids* **24** 055106
[21] Poorte R E G and Biesheuvel A 2002 Experiments on the motion of gas bubbles in turbulence generated by an active grid *J. Fluid Mech.* **461** 127
[22] Tagawa Y, Martínez Mercado J, Prakash V N, Calzavarini E, Sun C and Lohse D 2012 Three-dimensional Lagrangian Voronoi analysis for clustering of particles and bubbles in turbulence *J. Fluid Mech.* **693** 201
[23] Martínez Mercado J, Chehata Gómez D, van Gils D, Sun C and Lohse D 2010 On bubble clustering and energy spectra in pseudo-turbulence *J. Fluid Mech.* **650** 287
[24] Rensen J, Luther S and Lohse D 2005 The effects of bubbles on developed turbulence *J. Fluid Mech.* **538** 153
[25] Takagi S and Matsumoto Y 2011 Surfactant effects on bubble motion and bubbly flows *Annu. Rev. Fluid Mech.* **43** 615
[26] Takagi S, Ogasawara T, Fukuta M and Matsumoto Y 2009 Surfactant effect on the bubble motions and bubbly flow structures in a vertical channel *Fluid Dyn. Res.* **41** 065003
[27] Peng T 2005 Detect circles with various radii in grayscale image via Hough transform *MATLAB Central File Exchange* **9168** available at http://www.mathworks.com/matlabcentral/fileexchange/9168-detect-circles-with-various-radii-in-grayscale-image-via-hough-transform
[28] Gonzalez R C, Woods R E and Eddins S L 2004 *Digital Image Processing Using MATLAB* (Upper Saddle River, NJ: Pearson Education)
[29] Ballard D H 1981 Generalizing the Hough transform to detect arbitrary shapes *Pattern Recognit.* **13** 111
[30] Calzavarini E, Volk R, Leveque E, Pinton J-F and Toschi F 2012 Impact of trailing wake drag on the statistical properties and dynamics of finite-sized particle in turbulence *Physica* D **241** 237